

# Color Cast Dependent Image Dehazing via Adaptive Airlight Refinement and Non-linear Color Balancing

Sobhan Kanti Dhara, Mayukh Roy, Debasish Sen, and Prabir Kumar Biswas

**Abstract**—Hazy images suffer from low visibility since the light gets scattered as it passes through various atmospheric particles. Moreover, such images are prone to color distortion, particularly in real weather conditions like sandstorms. In this letter, an effective dehazing technique is proposed using weighted least squares filtering on dark channel prior and color correction that involves automatic detection of color cast images. We show that the spread of the hue in a hazy image can differentiate a color cast image from a non-cast one. We propose a measure using the same for categorizing hazy images as cast and non-cast ones. Our novel color correction is performed by color balancing using a non-linear transformation followed by a cast-adaptive airlight refinement. Subjective and quantitative evaluations show that our method outperforms the state-of-the-art. It removes cast satisfactorily and reduces haze substantially while maintaining the naturalness of the image. Moreover, it produces visually pleasing images without halo artifacts.

**Index Terms**—Image dehazing, airlight refinement, color cast removal, dark channel prior, weighted least squares filtering.

## I. INTRODUCTION

**H**AZE is a phenomenon in which light gets scattered by various particles like smoke, fog, mist and aerosols present in the atmosphere. This significantly degrades images by hampering the image visibility, contrast, vividness and color [1]–[6], affecting various image processing applications like surveillance, automatic driving systems etc.

Most of the recent single image based dehazing techniques like [1], [2], [7] aim at image dehazing based on the Koschmieder's optical model [8], and estimate the transmission map and the airlight based on various priors [1], [7]. Among different prior, the dark channel prior (DCP) [1] is a popular one. Employing this prior to calculate the scene radiance leads to the formation of halo artifacts, which can be removed by various refinement techniques like guided filter [2], weighted guided filter [9] etc. However, most of these methods either have a high time complexity or do not perform well in removing halo artifacts [10]. The success of deep learning in computer vision tasks led to a plethora of deep learning-based dehazing approaches [5], [6], [11], [12]. Cai et al. [11] proposed an end-to-end convolution neural network (CNN) for image dehazing. Zhang et. al proposed dehazing network which estimates the transmission map using generative adversarial network (GAN) [5]. Pang et. al. [6] proposed GAN based image dehazing network which estimates both transmission map and airlight. Liu et al. [12] proposed an attention based multi-scale model for image dehazing.

The authors are associated with Dept. of Electronics and Electrical Communication Engineering, Indian Institute of Technology, Kharagpur, India. Corresponding author: Debasish Sen (e-mail: dsen@ece.iitkgp.ac.in). The first two authors share equal contribution.

A real weather hazy image is prone to color cast in the presence of different suspended particles like sands, chemical substances [2], [4] etc. The generic techniques like the ones mentioned above, fail to restore the actual color of the scene. Thus, dehazing of an image becomes more challenging in images affected by color cast. Huang et. al. [4] addressed cast due to sandstorm during image dehazing and proposed a solution by computing the difference between the means of the red channel and the other channels. Tarel et. al. [13] proposed color balancing in haze removal framework for making the fog pure white. Ancuti et. al. [14] generated multiple images from input through color rendition and then fused them through multi-scale image fusion for dehazing. They take one of the inputs as a white balanced image. Choi et. al. [15] extended the idea including fog density weight for fog-density aware haze removal. Peng et. al. [16] proposed single image restoration in the presence of color cast using scene radiance estimation and correction. They use regression to find out the relation between RGB intensity and scene depth. The authors of [16] performed color cast aware single image dehazing in [2], where color correction is done through saturation correction. Correction in color cast hazy images is required, but it would be unnecessary for non-cast ones which may result in degradation. So, [2] proposes hazy image classification which is based on the extent of 'diffusion of hue probability' [2]. Santra et. al. [17] proposed CNN based patch quality comparator for image dehazing and showed that it could handle color cast. Recently, Yin et. al. [3] proposed color transferred CNNs to handle color cast while dehazing.

In this letter, we propose a dehazing approach, where:

- We suggest that dehazing should be performed considering whether an image is color cast or not. In this letter, we show that the spread of the hue in a hazy image can differentiate a color cast image from a non-cast one. We use the same to compute a decision boundary through classification error minimization for categorizing hazy images as cast and non-cast ones.
- We suggest that modification of pixel values based on Gray World assumption should be done in a non-linear fashion for color balancing. We propose a novel cast-adaptive non-linear transformation of the form  $I_c^\eta$  in each color channel ( $I_c$ ), where  $\eta$  ( $\leq 1$ ) corresponding to a channel is inversely related to its deviation from the Gray World assumption.
- We propose a novel cast-adaptive airlight refinement approach along with color balancing for color correction.
- We suggest the use of weighted least squares (WLS)



Fig. 1. Flowchart of the Proposed Method. Blue and red arrows are related to the flow for color cast and non-cast respectively.

framework for DCP refinement to ensure a dehazed image with no halo artifacts.

The rest of the letter is organized as follows. In Section II, our proposed approach is discussed in detail. Section III contains its subjective and quantitative comparison with the state-of-the-art. Section IV concludes the letter.

## II. PROPOSED METHOD

According to Koschmieder's Optical Model [8], the hazy image formation can be described by the following expression,

$$I(x) = J(x)t(x) + (1 - t(x))A \quad (1)$$

where  $I$  is the hazy image formed at  $x$ ,  $A$  is the airlight,  $J$  is the actual scene radiance, and  $t$  is the transmission map.  $t(x)$  is dependent on the distance of the object in the scene corresponding to the pixel  $x$ , from the camera.  $t$  is represented as  $t(x) = e^{-\beta d(x)}$ , where  $\beta$  is the attenuation factor and  $d(x)$  is the depth. A few intermediate outputs in our procedure to obtain  $J$  from  $I$  using (1) are shown in Fig. 1. The approach has six modules, namely classification, color balancing, DCP computation, airlight estimation and correction, transmission map estimation, and scene radiance computation.

### A. Hazy Image Classification as Color Cast or Non-cast

Hazy images can be categorized into two types: color cast and non-cast. We find that the spread of hue of an image is an important feature for identifying whether an image is cast or not and therefore, define a measure of the spread of hue as  $MOS = \frac{1}{MN} \sum_x \sum_y \delta(x, y)$ , where  $\delta = \min((\mu - h(x, y))^2, (1 - |\mu - h(x, y)|)^2)$ ,  $\mu$  is the mean hue,  $h(x, y) \in [0, 1]$  is the hue value at location  $(x, y)$  of an image of size  $M \times N$ .  $MOS$  defines the spread of hue considering its circularity nature. Fig. 2-A and Fig. 2-B show that color cast images usually have very small  $MOS$  and non-cast ones can have high  $MOS$ . We have generated the PDFs of  $MOS$  of 5700 cast and non-cast hazy images collected from flickr®. The PDFs of the two classes of images are shown in Fig. 2-C, where we see that the hue of the color cast images indeed has a very small  $MOS$ , while  $MOS$  of the non-cast images can vary widely with a very little probability of being small. We use classification error minimization to get a decision boundary as given below, based on which we classify an image as color cast or not. The classification error  $\epsilon_t$ , corresponding to a particular threshold  $t$  is given as:  $\epsilon_t = \sum_{x \in R_1} p(x|\omega_{nc}) + \sum_{x \in R_2} p(x|\omega_c)$ , where  $R_1$  and  $R_2$  are the cast (c) and non-cast (nc) regions formed based on a particular threshold;  $p(x|\omega_{nc})$  and  $p(x|\omega_c)$  are the class conditional probabilities for non-cast and cast images, respectively. The optimal threshold that we consider as the decision boundary is  $t_{opt} = \arg\min_t(\epsilon_t)$ , which, based on the images of Fig. 2-C, is 0.005 (MOS score).

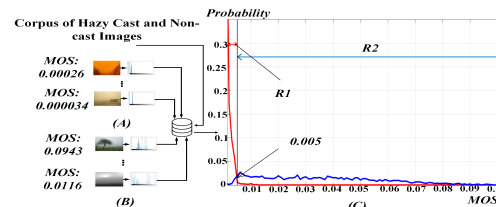


Fig. 2. A-Hue Histogram of Cast Image. B- Hue Histogram of Non-cast Image. C- Cast and Non-cast Image Classification. Blue and Red Graphs are the PDF of MOS of Cast Images and Non-cast Images Respectively.

### B. Color Balancing of the Color Cast Hazy Images

The Gray World assumption is that the mean reflectance is achromatic for natural scenes [18]. Due to computational simplicity and effectiveness, Gray World assumption or a modification of it for color balancing has been very popular. Such techniques linearly stretch the color channels ( $I_c$ ), which may either generate artifacts or limit color correction. The degree of correction for a particular channel pixel should be more if its intensity is less and should gradually decrease as intensity increases. A non-linear transformation of the form  $I_c^\eta$  is employed for the same. As Gray World assumption suggests that the mean reflectance is achromatic, we set  $\eta = \frac{\mu_c}{\mu_{max}}$  ( $\leq 1$ ), where  $\mu_c$  is the mean of the  $c^{\text{th}}$  channel of the image,  $\mu_{max} = \max_{i \in \{r,g,b\}} \mu_i$ . As image dehazing makes the dehazed image dimmer [1], we consider the maximum of the means (instead of the minimum or average) as it would cause the most increase in channel intensity, and therefore, the mean brightness. We generate a color balanced image  $I'$  from an input  $I$  through  $I'_c(x) = \min(I_c^\eta(x), \max_{i \in \{r,g,b\}} I_i(x))$ . The color balancing also helps in better estimation of DCP which is affected by the presence of color cast.

### C. DCP Calculation for all Hazy Images

The depth of the scene is estimated as the DCP [1]:  $D(y) = \min_{x \in \Omega(y)} \left( \min_{c \in \{r,g,b\}} I'_c(x) \right)$ , where  $\Omega$  is the patch around pixel  $y$  and  $I'$  is the color balanced image. For a non-cast,  $I' = I$ .

### D. Airlight Estimation and Refinement

1) *Airlight estimation for all images:* As per [1], we take the top 0.1% brightest pixels (defined as  $P_D^{0.1\%}$ ) in the DCP  $D$  and compute three airlight values for three channels ( $A_c$ ) as  $A_c = \frac{1}{|P_D^{0.1\%}|} \sum_{x \in P_D^{0.1\%}} I'_c(x)$ ,  $\forall c \in \{r, g, b\}$ , where  $I' = I$  is for non-cast images.

2) *Refinement for color cast images:* We find that color balancing alone is not sufficient for substantial color cast removal in cast images, and therefore, airlight refinement is also required. Now, lesser the discrepancy between a channel's airlight from the maximum of all airlights ( $A_r, A_g, A_b$ ), lesser should be the refinement. The airlight vector ( $[A_r, A_g, A_b]$ ) computed from the region corresponding to  $P_D^{0.1\%}$  in the DCP should ideally be achromatic for a non-cast image [19]. Further, the refinement should include the  $MOS$  score corresponding to  $P_D^{0.1\%}$  in the DCP, which determines the degree of color cast. Considering these factors, we define the refinement term,  $\alpha_c$  for a channel as  $\alpha_c = \left( \frac{A_{max}}{A_c} \right)^{\sqrt{\kappa_c}}$  where  $A_{max} = \max_{c \in \{r,g,b\}} A_c$ . The ratio  $\frac{A_{max}}{A_c}$ , which is a

TABLE I

NON-CAST AND COLOR CAST HAZY IMAGE CLASSIFICATION ACCURACY.		
Method	Non-Cast Hazy Image (%)	Color Cast Hazy Image (%)
Peng [2]	100	75.81
Ours	100	<b>91.46</b>

measure of deviation of the other channels from the casted channel, is used to maintain the achromatic nature of airlight for non-cast image. We choose the deviation from the maximum because airlight is supposed to be computed from the brightest region of the image corresponding to brightest region in DCP [1]. But use of the ratio alone causes color distortion specifically in the presence of higher color cast. As per section II-A, the *MOS* score is a measure of the degree of color cast. Hence, we introduce an exponent term based on the *MOS* score  $v$  as an attenuating factor in a manner that higher the color cast, higher will be the attenuation. The term  $\frac{A_{max}}{A_c}$  is attenuated by  $\kappa_c$ , which is given as  $\kappa_c = 2\sqrt{v}$ . The final airlight after refinement for a channel of a color cast image is obtained by updating,  $A_c = \frac{A_c}{\kappa_c}, \quad \forall c \in \{r, g, b\}$ .

#### E. Transmission Map Estimation and Scene Radiance Computation for All Hazy Images

The transmission map  $t$  is estimated like in [1]  $t_c(x) = 1 - \omega \frac{\Lambda(D)}{A_c}, \forall c \in \{r, g, b\}$ , where  $\omega$  is for preserving naturalness of the image. We consider  $\omega = 0.95$  like [1], [2].  $\Lambda$  represents the Weighted Least Squares (WLS) filtering as given in [20], which we use for refining the dark channel to get the transmission map. WLS distributes blurring near edges globally, reducing halo artifacts [20]. Finally, the scene radiance is computed from (1) as  $J_c(x) = A_c + \frac{I'_c(x) - A_c}{\max(t_0, t_c(x))}, \forall c \in \{r, g, b\}$ , where  $t_0 = 0.1$  like [1], [2] and  $I' = I$  for non-cast image.

### III. EXPERIMENTAL RESULTS AND DISCUSSION

We consider the dehazing techniques of He [1], Cai [11], Liu [12], Tarel [13], Choi [15], Santra [17], Yin [3] and Peng [2] for comparison. The results of these techniques are generated from the authors' codes with the specified parameters. We compare their results to the results generated by our algorithm (Ours), and also the results of our algorithm without airlight correction (Our (woac)), without color balancing (Our (wocb)), without both color balancing and airlight correction (Our (nc)), providing ablation study. Further, our approach of classifying cast and non-cast hazy images is compared to the classification technique of Peng [2]. We perform quantitative and subjective evaluations on three standard test databases, namely, LIVE [15] for real, SOTS [21], [22] for synthetically generated hazy images, O-HAZE [23] for haze machine generated hazy images along with the standard images of [2] and [4]. To generate synthetic haze in images, we follow (1), depth computation of [24], and take different values of airlight  $A$  and  $\beta$ . For non-cast images, we take  $\beta$  as 2, 3.5 and 5 to generate low, medium and high density haze, respectively. Further, single value of  $A$ , randomly chosen from {0.65, 0.72, 0.85}, is used for every channel of an image. For generating cast images, we select a yellow airlight used to generate yellow color cast hazy images in [2]. We also generate red and green color cast hazy images as those are also the commonly generated color cast in presence of haze [2]. For variety, we

generate hazy color cast images randomly choosing one among the three values of  $\beta$  mentioned earlier, and by randomly choosing one among the three airlights, which generates red, yellow or green cast.

In Table I, we show accuracies of classifying synthetic color cast hazy images from non-cast ones. The result shows that our technique outperforms the latest classification technique of [2] for color cast images and correctly classifies all the non-cast images like the technique of [2]. The measure of color cast by [2] is the number of connected components in the hue histogram considering the bins whose count is below a threshold. We compute MOS that determines the spread of hue without any threshold. Moreover, MOS computation considers the circular nature of hue possibly unlike [2].

We perform quantitative evaluation on images with synthetic haze based on four measures, namely, PSNR for pixel-wise difference based image quality, SSIM [25] for perceptual image quality, CIEDE2000 [26] for color difference and FADE [15] for haze density measure. Higher values of PSNR and SSIM and lower values of CIEDE2000 and FADE measures imply better performance. We generate two types of images- cast images with varying haze densities and non-cast images with the three densities given by  $\beta$  of haze as discussed earlier. Table II shows the results for non-cast images having three different haze densities and Table III shows the same for cast images with varying haze densities. We see that our technique outperforms the state-of-the-art in terms of all measures, for low, medium and high haze as well as in color cast conditions. As all the non-cast hazy images are classified correctly, no color correction is performed in the cases of the last 4 columns of Table II resulting in the same values. So, the better performance of our approach in non-cast hazy images is primarily due to better transmission map estimation using WLS.

Further, we present results of different variations of our approach with and without classification on the equal number of cast and non-cast hazy images generated using randomly chosen  $\beta$  and airlights in Table IV. Without classification, color balancing and/or airlight refinement will always be applied. Better results are obtained using classification. Here, 'Our (nc)' with no correction is the same in both the cases.

For real-life images, we perform no-reference quantitative analysis on LIVE database and use the measures BLIINDS-2 [27], BRISQUE [28], Gradient Ratio [7] and FADE [15] to evaluate the results. Table V gives the average values of the measures on the dehazed images for all the approaches considered. Lower the value of a measure, better is the performance, except Gradient ratio, where it is the opposite. As evident from Table V, the proposed technique is better in dehazing as suggested by FADE, and produces perceptually pleasing results as per BLIINDS-2 and BRISQUE. Further, our technique gives significantly higher Gradient Ratio, which implies that more edge details are preserved after dehazing [7].

Figs. 3 and 4 respectively show results on synthetic and real world non-cast (3.A and 4.A) and cast (3.B-3.D and 4.B-4.D) hazy images. These images are classified correctly by both ours and Peng [2] approaches. From Fig. 3.A, we see that our technique outperforms the rest in removing haze and



Fig. 3. Qualitative Results on Images with Synthetic Haze. ‘nc’ Stands For No Color Correction, ‘woac’ Stands for Without Airlight Correction and ‘wocb’ stands for without Color Balancing. The cropped regions from the red box area in the images are shown for thorough comparison.

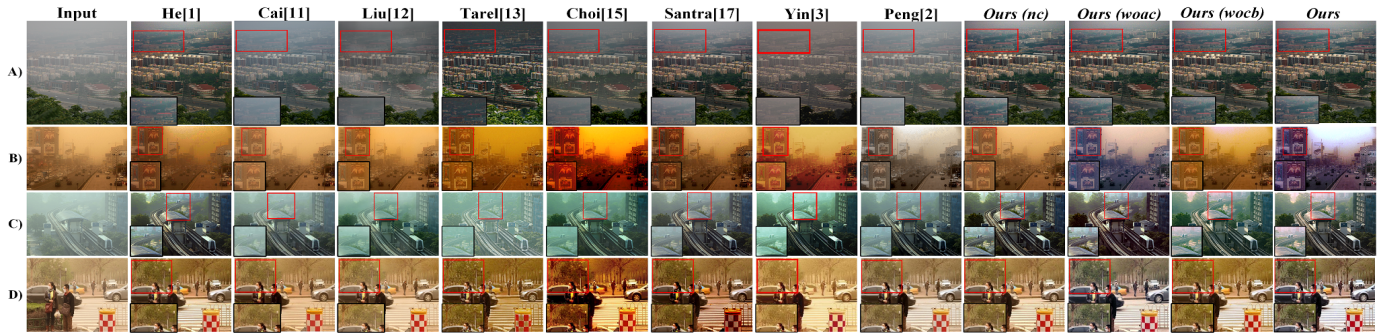


Fig. 4. Qualitative Results on Real Hazy Images. ‘nc’, ‘woac’, ‘wocb’ and the red boxes for the same reason as in Fig. 3.

TABLE II

QUANTITATIVE EVALUATION ON IMAGES WITH SYNTHETIC NON-CAST HAZE. ‘OC’ STANDS FOR WITH OUR CLASSIFIER, ‘NC’ STANDS FOR NO COLOR CORRECTION, ‘WOAC’ FOR WITHOUT AIRLIGHT CORRECTION AND ‘WOCB’ FOR WITHOUT COLOR BALANCING.

Measure	Haze	He [1]	Cai [11]	Liu [12]	Tarel [13]	Choi [15]	Santra [17]	Yin [3]	Peng [2]	Peng [2] (oc)	Ours (nc)	Ours (woac)	Ours (wocb)	Ours
PSNR/ SSIM	Low	17.33/ 0.82	16.84/ 0.77	16.73/ 0.82	13.2/ 0.74	14.46/ 0.75	17.53/ 0.81	15.09/ 0.69	17.07/ 0.81	17.07/ 0.81	<b>17.92/ 0.87</b>	<b>17.92/ 0.87</b>	<b>17.92/ 0.87</b>	<b>17.92/ 0.87</b>
CIEDE2000/ FADE	$\beta = 2$	9.99/ 0.96	10.57/ 1.5	10.37/ 1.1	16.21/ 0.97	13.7/ 0.98	9.67/ 0.79	13.8/ 0.82	10.4/ 0.97	10.4/ 0.97	<b>9.17/ 0.59</b>	<b>9.17/ 0.59</b>	<b>9.17/ 0.59</b>	<b>9.17/ 0.59</b>
PSNR/ SSIM	Medium	16.66/ 0.75	12.61/ 0.56	11.92/ 0.59	11.78/ 0.61	12.1/ 0.55	14.6/ 0.66	13.2/ 0.55	14.67/ 0.66	14.67/ 0.66	<b>17.3/ 0.79</b>	<b>17.3/ 0.79</b>	<b>17.3/ 0.79</b>	<b>17.3/ 0.79</b>
CIEDE2000/ FADE	$\beta = 3.5$	10.73/ 1.44	18.37/ 2.58	19.18/ 1.66	19.98/ 1.54	18.75/ <b>1.1</b>	13.9/ 1.12	16.96/ 1.11	14.1/ 1.3	14.1/ 1.3	<b>9.9/ 1.1</b>	<b>9.9/ 1.1</b>	<b>9.9/ 1.1</b>	<b>9.9/ 1.1</b>
PSNR/ SSIM	High	14.01/ 0.62	10.76/ 0.44	9.7/ 0.44	10.9/ 0.5	11.26/ 0.44	11.8/ 0.52	11.99/ 0.45	12.56/ 0.53	12.56/ 0.53	<b>14.32/ 0.65</b>	<b>14.32/ 0.65</b>	<b>14.32/ 0.65</b>	<b>14.32/ 0.65</b>
CIEDE2000/ FADE	$\beta = 5$	15.11/ 1.83	23.43/ 3.85	25.4/ 2.81	22.8/ 2.1	21.4/ 3.18	20.02/ 2.3	19.5/ 1.4	18.4/ 1.78	18.4/ 1.78	<b>14.5/ 1.2</b>	<b>14.5/ 1.2</b>	<b>14.5/ 1.2</b>	<b>14.5/ 1.2</b>

TABLE III

QUANTITATIVE EVALUATION ON IMAGES WITH SYNTHETIC CAST HAZE. OC, NC, WOAC AND WOCB SAME AS IN TABLE II.

Measure	He [1]	Cai [11]	Liu [12]	Tarel [13]	Choi [15]	Santra [17]	Yin [3]	Peng [2]	Peng [2] (oc)	Ours (nc)	Ours (woac)	Ours (wocb)	Ours
PSNR/ SSIM	14.12/ 0.44	11.89/ 0.28	11.5/ 0.22	10.7/ 0.39	10.3/ 0.18	14.1/ 0.38	12.1/ 0.22	13.7/ 0.37	13.85/ 0.38	13.6/ 0.27	14.1/ 0.39	13.7/ 0.37	<b>14.22/ 0.52</b>
CIEDE2000/ FADE	19.55/ 1.19	25.44/ 1.94	27.74/ 1.4	30.7/ 1.21	28.3/ <b>1.1</b>	19.8/ 1.12	24.5/ 1.11	20.3/ 1.34	19.8/ 1.36	23.9/ 1.15	19.6/ 1.13	22.78/ 1.12	<b>19.2/ 1.1</b>

also the color contrast is maintained after dehazing. Others do not significantly remove haze from high haze regions. The results of Figs. 3.B-3.D show that our technique is the closest to the ground truth (GT) than the other techniques. [1], [3], [11]–[13], [15] do not remove the cast sufficiently. [15] over-saturates the color. [2], [17] give good results but do not work satisfactorily at high color cast regions. Fig. 4.A shows that our technique removes haze the most. Results of [3], [15] suffer from over-saturation. The techniques also do not significantly dehaze the high haze regions. Further, our results retain the brightness of the scene, unlike that of [13]. From Figs. 4.B–4.D, we see that our technique retains the object color, while substantially removing the cast from the scene (as can be seen from the cropped regions). [2] does well in color cast removal but the dehazed image suffers from color loss. Our technique gives sharper results with very high clarity and low haze in comparison to all the other techniques. Our technique removes color cast without over-saturation and color loss. When the amount of color cast and/or haze increases, our technique still performs significantly well in dehazing and color cast removal.

Table VI presents the results on O-HAZE [23] database. We see that our result outperforms all methods in terms of PSNR, SSIM, CIEDE2000 and all but [3] in terms of FADE.

The ablation study based on both quantitative and subjective comparison among the ‘Ours (nc)’, ‘ours (woac)’, ‘Ours (wocb)’ and ‘Ours’ approaches show that our color balancing and airlight refinement modules contribute to the performance individually during haze removal in color cast images. The gradual improvement in all the measures, including CIEDE2000, which quantifies the color difference, shows the importance of each module. The same is evident from the subjective results, where we see that the addition of each module helps to remove the color cast, and finally, our technique with all color correction modules performs the best.

Table VII compares the computation times, where our technique outperforms the CPU based ones except [2] for all image sizes. The techniques are run either using MATLAB in CPU having Intel i5-3.30GHz, 16 GB RAM or Python in Nvidia Tesla K80 GPU.

Fig. 5 presents the performance of object detection for autonomous driving by the state-of-the-art technique Squeezedet [29] on an image from KITTI database [30], its hazy version and the dehazed output by ‘Ours’. Results show that dehazing improves the performance over the hazy image and leads to the detection of all the objects detected in the original image.

TABLE IV  
RESULTS WITH AND WITHOUT CLASSIFICATION ON EQUAL NUMBER OF IMAGES WITH SYNTHETIC COLOR CAST AND NON-CAST HAZE.

Measure	With Classification			Without Classification		
	Ours (nc)	Ours (woac)	Ours	Ours (nc)	Ours (woac)	Ours
PSNR/ SSIM	14.95/ 0.52	15.2/ 0.58	15.01/ 0.57	15.3/ 0.64	14.95/ 0.52	15.19/ 0.55
CIEDE2000/ FADE	17.72/ 1.02	15.57/ 1.01	17.16/ 1.00	15.36/ 0.99	17.72/ 1.02	15.63/ 1.01

TABLE V

QUANTITATIVE EVALUATION ON REAL HAZY IMAGES. OC, NC AND WOAC SAME AS IN TABLE II.

Measure	He [1]	Cai [11]	Liu [12]	Tarel [13]	Choi [15]	Santra [17]	Yin [3]	Peng [2]	Peng [2] (oc)	Ours (nc)	Ours (woac)	Ours (wocb)	Ours
BLINDS-2/ BRISQUE	17.47/ 26.65	22.55/ 29.14	11.85/ 24.12	16.33/ 25.71	20.86/ 27.5	19.16/ 25.26	24.41/ 25.6	18.81/ 25.8	18.71/ 25.7	10.81/ 20.7	10.66/ 20.6	10.8/ 20.64	<b>10.18/ 20.5</b>
Grad. Ratio/ FADE	1.54/ 0.83	1.26/ 1.23	1.26/ 1.35	1.57/ 0.74	1.57/ 0.74	1.64/ 0.7	1.54/ 0.84	1.36/ 0.9	1.36/ 0.9	2.16/ 0.47	2.19/ 0.46	2.22/ 0.46	<b>2.23/ 0.44</b>

TABLE VI

QUANTITATIVE EVALUATION ON O-HAZE (TESTING+VALIDATION) DATABASE. OC, NC, WOAC AND WOCB SAME AS IN TABLE II.

Measure	He [1]	Cai [11]	Liu [12]	Tarel [13]	Choi [15]	Santra [17]	Yin [3]	Peng [2]	Peng [2] (oc)	Ours (nc)	Ours (woac)	Ours (wocb)	Ours
PSNR/ SSIM	16.77/ 0.49	16.42/ 0.49	17.53/ 0.48	14.81/ 0.45	15.69/ 0.38	17.84/ 0.52	16.7/ 0.49	16.51/ 0.47	16.57/ 0.48	16.56/ 0.46	17.29/ 0.55	16.71/ 0.46	<b>17.95/ 0.58</b>
CIEDE2000/ FADE	15.96/ 0.39	14.73/ 0.83	15.78/ 0.73	17.93/ 0.41	19.95/ 0.3	14.1/ 0.54	16.14/ <b>0.24</b>	16.58/ 0.41	16.24/ 0.41	17.24/ 0.32	14.43/ 0.32	16.81/ 0.32	<b>13.99/ 0.29</b>

TABLE VII

COMPUTATION TIME (SECONDS) OF DIFFERENT ALGORITHMS AT DIFFERENT SIZES. NC, WOAC, WOCB SAME AS IN TABLE II.

Resolution	Device	He [1]	Cai [11]	Liu [12]	Tarel [13]	Choi [15]	Santra [17]	Yin [3]	Peng [2]	Peng [2] (oc)	Ours (nc)	Ours (woac)	Ours (wocb)	Ours
320 × 240/ 640 × 480 960 × 540/ 1280 × 720	CPU	4.75/ 20.32 34.99/ 64.46	0.4/ 2.3 3.87/ 6.95	—	0.42/ 4.82 18.3/ 51.67	3.85/ 15.2 25.67/ 47.01	—	—	0.08/ 0.32 <b>0.67/ 1.49</b>	0.23/ 0.91 1.58/ 2.99	0.3/ 1.13 1.9/ 3.72	0.24/ 1.02 1.77/ 3.58	0.31/ 1.17 2.07/ 3.8	—
	GPU	—	—	—	—	—	3.99/ 11.11 22.3/ 37.99	2.96/ 2.96 2.96/ 2.96	—	—	—	—	—	—



Fig. 5. Objection Detection in Autonomous Driving by Squeezedet [29].

#### IV. CONCLUSION

This letter proposes an efficient dehazing framework based on the Koschmieder's optical model that includes novel color cast classification and correction modules. Correction is performed through cast-adaptive non-linear color balancing and airlight refinement. Our color cast classifier's performance is found to be better than the existing. Qualitative and quantitative analysis has shown that the proposed approach ensures maximum dehazing and color cast removal without significant halo artifacts and color modification, producing sharp dehazed images better than the state-of-the-art.

#### REFERENCES

- [1] K. He, J. Sun, and X. Tang, "Single image haze removal using dark channel prior," *IEEE Trans. on Pattern Analysis and Machine Intelligence*, vol. 33, no. 12, pp. 2341–2353, 2011.
- [2] Y. Peng, Z. Lu, F. Cheng, Y. Zheng, and S. Huang, "Image haze removal using airlight white correction, local light filter, and aerial perspective prior," *IEEE Trans. on Circuits and Systems for Video Technology*, vol. 30, no. 5, pp. 1385–1395, 2020.
- [3] J. Yin, Y. Huang, B. Chen, and S. Ye, "Color transferred convolutional neural networks for image dehazing," *IEEE Trans. on Circuits and Systems for Video Technology*, pp. 1–1, 2019.
- [4] S. Huang, B. Chen, and W. Wang, "Visibility restoration of single hazy images captured in real-world weather conditions," *IEEE Trans. on Circuits and Systems for Video Technology*, vol. 24, no. 10, pp. 1814–1824, 2014.
- [5] H. Zhang, V. Sindagi, and V. M. Patel, "Joint transmission map estimation and dehazing using deep networks," *IEEE Trans. on Circuits and Systems for Video Technology*, 2019.
- [6] Y. Pang, J. Xie, and X. Li, "Visual haze removal by a unified generative adversarial network," *IEEE Trans. on Circuits and Systems for Video Technology*, vol. 29, no. 11, pp. 3211–3221, 2019.
- [7] T. M. Bui and W. Kim, "Single image dehazing using color ellipsoid prior," *IEEE Trans. on Image Processing*, vol. 27, no. 2, pp. 999–1009, 2018.
- [8] H. Koschmieder, "Theorie der horizontalen sichtweite," *Beitrage zur Physik der freien Atmosphare*, pp. 33–53, 1924.
- [9] Z. Li, J. Zheng, Z. Zhu, W. Yao, and S. Wu, "Weighted guided image filtering," *IEEE Trans. on Image Processing*, vol. 24, no. 1, pp. 120–129, 2014.
- [10] Z. Li and J. Zheng, "Edge-preserving decomposition-based single image haze removal," *IEEE Trans. on Image Processing*, vol. 24, no. 12, pp. 5432–5441, 2015.
- [11] B. Cai, X. Xu, K. Jia, C. Qing, and D. Tao, "Dehazenet: An end-to-end system for single image haze removal," *IEEE Trans. on Image Processing*, vol. 25, no. 11, pp. 5187–5198, 2016.
- [12] X. Liu, Z. Ma, Z. Shi, and J. Chen, "Griddehazenet: Attention-based multi-scale network for image dehazing," in *IEEE International Conf on Computer Vision*, pp. 7314–7323, 2019.
- [13] J. Tarel and N. Hautire, "Fast visibility restoration from a single color or gray level image," in *IEEE International Conference on Computer Vision*, pp. 2201–2208, 2009.
- [14] C. O. Ancuti and C. Ancuti, "Single image dehazing by multi-scale fusion," *IEEE Trans. on Image Processing*, vol. 22, no. 8, pp. 3271–3282, 2013.
- [15] L. K. Choi, J. You, and A. C. Bovik, "Referenceless prediction of perceptual fog density and perceptual image defogging," *IEEE Trans. on Image Processing*, vol. 24, no. 11, pp. 3888–3901, 2015.
- [16] Y. Peng, K. Cao, and C. P. Cosman, "Generalization of the dark channel prior for single image restoration," *IEEE Trans. on Image Processing*, vol. 27, no. 6, pp. 2856–2868, 2018.
- [17] S. Santra, R. Mondal, and B. Chanda, "Learning a patch quality comparator for single image dehazing," *IEEE Trans. on Image Processing*, vol. 27, no. 9, pp. 4598–4607, 2018.
- [18] G. Buchsbaum, "A spatial processor model for object colour perception," *Journal of the Franklin institute*, vol. 310, no. 1, pp. 1–26, 1980.
- [19] F. Gasparini and R. Schettini, "Color correction for digital photographs," in *International Conference on Image Analysis and Processing*, pp. 646–651, 2003.
- [20] Z. Farbman, R. Fattal, D. Lischinski, and R. Szeliski, "Edge-preserving decompositions for multi-scale tone and detail manipulation," *ACM Trans. Graph.*, vol. 27, no. 3, pp. 110, 2008.
- [21] "SOTS," [https://www.dropbox.com/s/y6jupfvitv0dx5w/SOTS.zip?dl=0&file\\_subpath=%2FSOTS%2Foutdoor%2Fgt](https://www.dropbox.com/s/y6jupfvitv0dx5w/SOTS.zip?dl=0&file_subpath=%2FSOTS%2Foutdoor%2Fgt).
- [22] B. Li, W. Ren, D. Fu, D. Tao, D. Feng, W. Zeng, and Z. Wang, "Benchmarking single-image dehazing and beyond," *IEEE Trans. on Image Processing*, vol. 28, no. 1, pp. 492–505, 2019.
- [23] Codruta O Ancuti, Cosmin Ancuti, Radu Timofte, and Christophe De Vleeschouwer, "O-haze: a dehazing benchmark with real hazy and haze-free outdoor images," in *IEEE Conference on Computer Vision and Pattern Recognition Workshops*, pp. 754–762, 2018.
- [24] Z. Li and N. Snavely, "Megadepth: Learning single-view depth prediction from internet photos," in *IEEE Conference on Computer Vision and Pattern Recognition*, pp. 2041–2050, 2018.
- [25] Z. Wang, A. C. Bovik, H. R. Sheikh, E. P. Simoncelli, et al., "Image quality assessment: from error visibility to structural similarity," *IEEE Trans. on Image Processing*, vol. 13, no. 4, pp. 600–612, 2004.
- [26] G. Sharma, W. Wu, and E. Dalal, "The ciede2000 color-difference formula: Implementation notes, supplementary test data, and mathematical observations," *Color Research & Appl.*, vol. 30, pp. 21 – 30, 2005.
- [27] M. A. Saad, A. C. Bovik, and C. Charrier, "Blind image quality assessment: A natural scene statistics approach in the dct domain," *IEEE Trans. on Image Processing*, vol. 21, no. 8, pp. 3339–3352, 2012.
- [28] A. Mittal, A. K. Moorthy, and A. C. Bovik, "No-reference image quality assessment in the spatial domain," *IEEE Trans. on Image Processing*, vol. 21, no. 12, pp. 4695–4708, 2012.
- [29] B. Wu, F. Iandola, P. H. Jin, and K. Keutzer, "Squeezedet: Unified, small, low power fully convolutional neural networks for real-time object detection for autonomous driving," in *IEEE Conference on Computer Vision and Pattern Recognition Workshops*, pp. 129–137, 2017.
- [30] "KITTI," <http://www.cvlibs.net/datasets/kitti/>.